Journal of Instrumentation

Pulse shape discrimination performance of a pixelated plastic scintillator (EJ-299-34) for a coded-aperture based dual particle imaging system

Published by IOP Publishing for Sissa Medialab

Received: *May 31, 2019*
Revised: *July 4, 2019*
Accepted: *July 15, 2019*
Published: *July 25, 2019*

Pulse shape discrimination performance of a pixelated plastic scintillator (EJ-299-34) for a coded-aperture based dual particle imaging system

M.J. Cieślak,[a,1] **K.A.A. Gamage,**[b] **R. Glover**[c] **and C.J. Taylor**[a]

[a] *Department of Engineering, Lancaster University, Lancaster, LA1 4YW, U.K.*
[b] *School of Engineering, University of Glasgow, Glasgow, G12 8QQ, U.K*
[c] *Radiometric Systems Group, Sellafield Ltd, Seascale, CA20 1PG, U.K.*

E-mail: m.cieslak@lancaster.ac.uk

Abstract: The pulse shape discrimination performance of a pixelated organic plastic scintillator has been investigated. The scintillator has been built using 169 plastic scintillator blocks (arranged into a 13×13 square array) of $2.8 \times 2.8 \times 15\,\mathrm{mm}^3$ each. The scintillator was coupled with a single-channel photomultiplier tube. The scintillator was exposed to a mixed-field environment provided by ^{252}Cf and its pulse shape discrimination capabilities are presented in this paper. Initial results revealed that a 150 MS/s digitising system was insufficient to separate neutrons from gamma-ray photons. Therefore, the experiment was repeated with a 500 MS/s system, which provided improved pulse shape discrimination performance. In order to validate the performance of the pixelated plastic scintillator, it was compared to that of a cylindrical plastic sample. Tests were also carried out in moderated neutron and gamma-ray fields of ^{252}Cf. The results indicate that acceptable levels of pulse shape discrimination are obtained for the case of a pixelated scintillator, when the higher sampling rate digitiser was used.

Keywords: Gamma detectors (scintillators, CZT, HPG, HgI etc); Neutron detectors (cold, thermal, fast neutrons); Particle identification methods; Scintillators, scintillation and light emission processes (solid, gas and liquid scintillators)

[1] Corresponding author.

https://doi.org/10.1088/1748-0221/14/07/P07017

2019 JINST 14 P07017

Contents

2019 JINST 14 P07017

1 Introduction

Efficient and effective methods of radiation detection and imaging are highly desirable in numerous application areas, such as nuclear medicine, nuclear power generation, nuclear proliferation, nuclear decontamination and decommissioning. Depending on the information that is sought, different detection methods can be applied. For instance, X-ray imaging can be utilised for detecting the metallic parts of an item under investigation. However, if neutron imaging is applied to investigate the same item, the plastic parts of the item can be explored [1]. This is because distinctive targets interact in different ways as a result of exposure to varying radiation fields. Hence, combined X-ray and neutron imaging could provide a complementary solution for border control systems.

In a similar way, various radiation types are used in medicine e.g. ^{99m}Tc can be used to detect cancerous cells in a patient's body. As ^{99m}Tc is a human made gamma-ray emitter, it produces a specific gamma-ray field (photon energy of 140 keV) that can be detected using an appropriate gamma-ray imaging system. As its half-life is only 6.0058 hours, this approach allows enough time to produce an image of a patient's body and to track cancerous cells. Furthermore, its exposure time is short enough to keep the patient's absorbed dose low [2]. This is an example of a very specific application of radiation imaging i.e. when the produced radiation field is known.

For the application areas described above, in most cases the expected radiation field to be detected is known, whereas for nuclear decontamination and decommissioning applications it is generally unknown. During this final stage of a nuclear power plant's life, the local infrastructure, as well as the surrounding grounds, are required to be characterised in order to restore the area to

a safe state. It is often difficult to judge what type of radiation, or specific spectrum of a certain radiation type, would be envisaged in a particular area. The information required to infer the type of radioactive isotope is often found in its gamma-ray or neutron spectrum [3]. Hence, it is beneficial to understand whether traces of these radiation types are present in the area of investigation.

1.1 Scintillator based detectors used in nuclear decommissioning applications

Particle detectors suitable for nuclear decommissioning applications in mixed-field environments are required to be sensitive to both neutrons and gamma-ray photons. Over the years, organic liquid scintillators have been established as one of the most popular choices for mixed-field applications [4, 5]. This is primarily due to their good neutron/gamma-ray separation quality and reasonable spectroscopic response. However, they are only sensitive to fast neutrons. Moreover, liquid scintillators are characterised by high toxicity, and some cocktails also have a low flash-point [6]. Hence, they are often inappropriate for use in sensitive industrial environments, such as nuclear decommissioning facilities.

Such limitations have been gradually addressed by research into plastic organic scintillators. These detectors are not toxic and the risk of spillage is fully alleviated. However, only recently has a plastic scintillator been developed whose pulse shape discrimination (PSD) performance is comparable to an EJ-309 liquid detector [7]. Furthermore, in a similar manner to organic liquids, plastic scintillators have been doped with ^{10}B and ^{6}Li to allow thermal neutron detection [8, 9]. Plastic scintillators can also be straightforwardly formed into array blocks. However, in regard to PSD performance, stilbene crystal is far superior when compared to liquid and plastic scintillators.

Stilbene and anthracene represent some of the oldest scintillation crystals that have been widely used. Stilbene has been broadly recognised as the preferred choice in neutron/gamma separation applications, due to its high particle discrimination quality. However, the crystal was difficult to grow and its production was only viable in small sizes (< 10 cm) until recently [3]. A relatively new method of growing the crystal has enabled researchers to go beyond the 10 cm limit and improve its light output [10]. Continuous improvements have led the stilbene crystal to offer far superior PSD performance when compared to plastic and liquid counterparts [11]. The manufacturing cost is however still high which makes building large stilbene detectors very expensive.

In order to improve the sensitivity of the detector across a greater energy spectrum, new methods of particle detection are sought. One of the recently proposed methods is a composite detector, where Cs_2LiYCl_6(CLYC), which is characterised by an excellent energy response and thermal neutron detection, is incorporated into a PSD capable plastic scintillator [12]. Such a scintillator is capable of separating thermal and fast neutrons, as well as gamma-ray events, that are induced in both the plastic and CLYC scintillators [13]. The downside of this approach lies in the detector size, as the composite is required to be sufficiently large so as to incorporate the inorganic scintillator inside.

Unfortunately, a large detector size is often a problem when nuclear decommissioning applications are considered. The areas to be interrogated are likely to be difficult to access and the space available for equipment deployment is scarce. Therefore, in the present article, we present some initial characterisation results of a small scale pixelated organic plastic scintillator (EJ-299-34). The overall dimensions of the scintillator, $39.52 \times 39.52 \times 15\,\text{mm}^3$, make it suitable for the intended application. Furthermore, the pixelated design, as well as a single pixel size of $2.8 \times 2.8 \times 15\,\text{mm}^3$,

2019 JINST 14 P07017

allows the scintillator to be matched to readily available pixelated photo detectors; in particular, a Position Sensitive Photomultiplier Tube (PSPMT) or a Silicon Photomultiplier (SiPM) can be utilised. Given the dimensions of the scintillator's single pixel, a one-to-one match can be found for the plastic scintillator. This characteristic is of vital importance when a sensitive detector is considered for coded-aperture based applications, as here.

1.2 Coded-aperture based radiation detectors

Coded-aperture based imaging is used to enhance the resolution of the reconstructed image, in comparison to conventional radiation imaging approaches, such as use of single opening collimators. As evidenced through extensive research conducted with gamma-ray detectors, higher lateral resolution allows the exposure time to be reduced [14]. However, in order to exploit the potential of a coded-aperture based approach, the location of the interaction within the scintillator must be reliably inferred. In particular, the direct matching of the pixel size between the scintillator and the photodetector can improve the process of interaction localisation.

Single particle detectors (X-ray and gamma-ray photons) utilising coded-aperture imaging methods have been thoroughly investigated [15–17]. A range of readily available pixelated inorganic scintillators, such as the CsI(Tl) scintillator, provide excellent energy resolution and can also be used to improve the spatial resolution due to their pixelated design [18]. There have been attempts to use pixelated detectors for fast neutron detection [19, 20]. However, the latter designs are based on a large scale approach and are not practical for nuclear decommissioning applications, which require more easily portable and deployable systems. Moreover, the systems described by references [19, 20] do not follow a one-to-one approach in regard to scintillator pixel and photodetector pixel dimensions.

1.3 Organic pixelated plastic scintillator EJ-299-34

The present article considers the suitability of the EJ-299-34 (produced by Eljen Technology) scintillator for neutron/gamma detection using PSD, based on experimental work performed with a ^{252}Cf radioactive source. Various digitising systems are used to comprehensively investigate the requirements of this novel scintillator. In particular, following on from previously performed work with FPGA based 150 MS/s and 500 MS/s digitising systems [21], these two devices were similarly used to analyse PSD performance here. To the authors knowledge, this is the first time that an analysis of the PSD performance of an organic pixelated plastic scintillator of this size scale has been reported. The scintillator was designed so that it can match currently available pixelated photodetectors, such as the Hamamatsu H9500 PSPMTs or SensL series-J SiPMs. It was further customised to address a previously performed MCNP based simulation study of the coded-aperture based neutron/gamma imaging system [22]. The pixelated scintillator comprises 169 scintillator blocks arranged into a 13 × 13 array, as shown in figure 1. All the scintillator blocks are optically isolated from one another through ^{TM}ESR reflective tape to provide up to 98% isolation.

Hence, a key objective of the present work is to assess the particle separation capability of the pixelated plastic scintillator (EJ-299-34), based on experimental work performed at Lancaster University, U.K.. A second contribution is the comparison of the scintillator's PSD performance in regard to the sampling frequency of the digitiser. For this purpose, FPGA based digitiser systems of different sampling frequency were used — 150 MS/s and 500 MS/s. In each case, the performance

2019 JINST 14 P07017

of the digitiser was verified with a cylindrical PSD plastic scintillator sample obtained from LLNL in 2016, which was previously tested [21]. Section 2 of the article describes the methodology and materials utilised in this work. This is followed in section 3 by presentation of the results. The findings are discussed in section 4, with the conclusions presented in section 5.

2 Methodology

Both neutrons and gamma-ray photons are examples of uncharged particles. Hence, they do not undergo Coulomb interactions with electrons in materials. In organic scintillators, they interact primarily with ^{1}H atoms through elastic scattering with a proton (neutrons), and Compton scattering with an atomic electron (gamma-ray photons). Each of these interactions result in a fluorescence emitted in the scintillator that is proportional to the rate of energy loss of the interacting particle. The fluorescence emitted can be subsequently detected via a suitable photodetector, which produces pulses that reflect the particle's rate of energy loss. The difference in the pulse shape can be exploited to separate gamma-ray interactions from neutron events via PSD techniques [21].

There are numerous PSD methods that can be implemented in the digital domain [23, 24]. However, the most popularly used technique is a charge comparison method (CCM) that was originally implemented in the analogue domain [25]. It relies on the integration of the pulse over two specific intervals. The first integral (I_{long}) is calculated over the entirety of the pulse, and the second integral (I_{short}) is calculated over a specific period of the tail of the pulse, as the difference between the pulses is most pronounced in this region. Graphical illustration of this method is presented in figure 2.

The scintillator used in this study was based on organic pixelated plastic provided by Eljen Technology. The outer dimensions of the scintillator are $39.52 \times 39.52 \times 15\,\text{mm}^3$. The scintillator

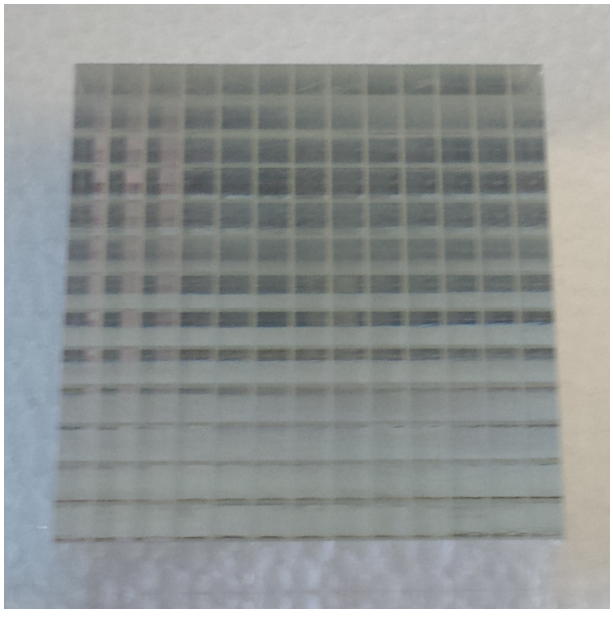

Figure 1. Organic pixelated plastic scintillator (EJ-299-34). There are 169 scintillator blocks of $2.8 \times 2.8 \times 15\,\text{mm}^3$, arranged into a 13×13 array.

2019 JINST 14 P07017

was subsequently coupled to an ET Enterprises 9107B photomultiplier tube (PMT). As the diameter of the PMT (25 mm) is smaller the outer dimensions of the pixelated plastic, appropriate light guide and EJ-550 silicone grease were used to provide optimal photon transfer. The PMT's sensitive area was placed at the centre of the pixelated plastic sample. A light-proof enclosure was placed around the scintillator-PMT assembly. The PMT was connected to a positive high voltage power supply of 850 V.

The assembly comprising the scintillator and the PMT was connected in turn to two FPGA based digitisers to infer its PSD potential. The first experiment was performed with a 14-bit resolution, 150 MS/s "raw data" digitiser. This collected 28 samples for every triggered pulse (every 6.67 ns). It was subsequently replaced with a 12-bit resolution, 500 MS/s "raw data" digitiser, which collected 128 samples (every 2 ns) for every triggered pulse.

The PSD capabilities of the scintillator were assessed using a ^{252}Cf fission source that is normally stored in the centre of a water filled steel tank. The source is pneumatically moved to towards the edge of the tank and is placed approximately 20 cm away from the edge, when in an exposed position. The detector assembly (scintillator-PMT) was placed 15 cm away from the edge of the water tank, resulting in a total distance of 35 cm between the source and the front of the detector.

The same equipment (PMT, digitisers) and facilities were used to take measurements using the cylindrical plastic PSD sample. The sample (25 mm diameter, 25 mm thickness) was developed at the Lawrence Livermore National Laboratory (LLNL), U.S.A. — denoted by the LLNL number 5706. The results obtained with this sample were contrasted with those of the pixelated scintillator. Further information about this research sample can be found in authors' preceding work [26].

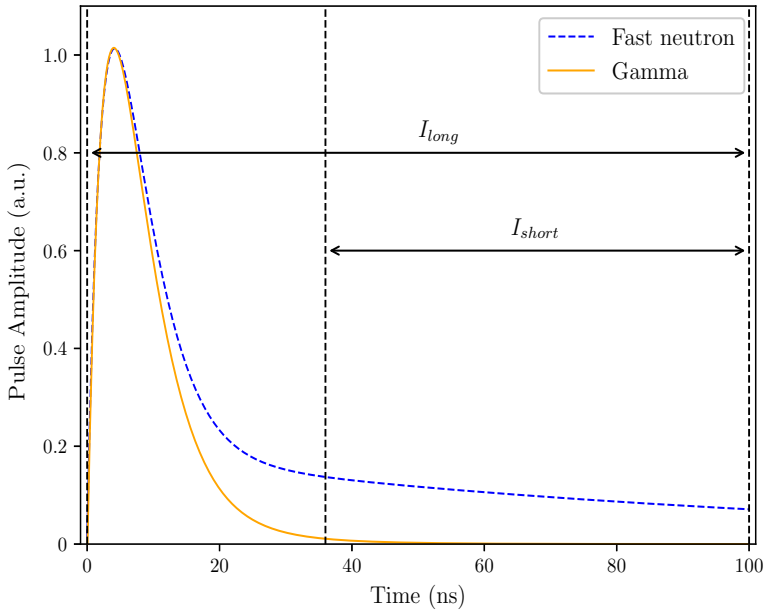

Figure 2. Illustration of the implementation of the pulse shape discrimination method used in this study. Long and short integrals used in CCM calculations are marked on the plot. Theoretical fast neutron and gamma-ray pulses were obtained based on the data from Knoll [3] and Zaitseva et al. [9].

2019 JINST 14 P07017

In subsequent experiments, a 5 cm thick modulation block made of lead was placed adjacent to the tank (as illustrated in figure 3), so that the single particle sensitivity of the detectors could be evaluated. The thickness of the lead block was subsequently increased to 10 cm to further block the gamma-ray field of ^{252}Cf. The final experiment was performed with a 9 cm thick high density polyethylene (HDPE) block placed adjacent to the tank in order to modulate the neutron field. In each case, the detector was exposed to the radioactive field for 30 minutes.

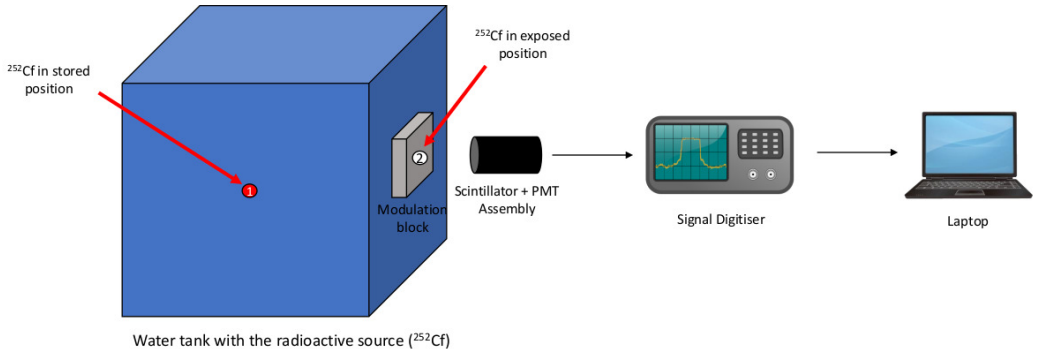

Figure 3. Schematic diagram of the experimental set-up. ^{252}Cf source is in the centre of a water-filled steel tank (position 1). During the experiments the source is moved to the edge of the tank (position 2).

3 Results

Initially both plastic scintillators were linked to the FPGA based 150 MS/s signal digitiser to collect the data. Each triggered pulse was processed through a bespoke pile-up rejection algorithm, where pulses with two peaks occurring within the same trigger window were rejected. There were 68,368 pulses accepted for the pixelated plastic sample and 80,955 for the cylindrical sample. Accepted pulses were used to plot CCM scatter plots as presented in figure 4, where (I_{short}) is depicted on the y-axis and (I_{long}) is depicted on the x-axis.

It can be noticed that only the PSD plastic sample (Figure 4b) is capable of separating the neutron events from gamma-ray photons interactions. Therefore, further quality assessment of particle separation is only considered for the PSD plastic sample, since the pixelated plastic scintillator sample is deemed not capable of performing neutron/gamma discrimination when the 150 MS/s digitiser is used for data collection.

Following a similar procedure, the scintillator and PMT assemblies were subsequently tested with the FPGA based 500 MS/s digitiser. Each triggered pulse was processed through the same rejection algorithm. There were 70,485 pulses accepted for the pixelated plastic scintillator, and 120,213 accepted for the cylindrical sample. Particle separation was also performed using CCM, as described above, and the resulting scatter plots are presented in figure 5.

In comparison to the results presented for the 150 MS/s digitiser (figure 4a), a significant improvement of PSD performance can be observed for the corresponding pixelated plastic scintillator plot when the 500 MS/s digitiser was used (figure 5a). However, it is still far inferior to the results obtained with the cylindrical sample. Nonetheless, it is deemed sufficient to be included in the separation quality analysis discussed in the following subsection.

2019 JINST 14 P07017

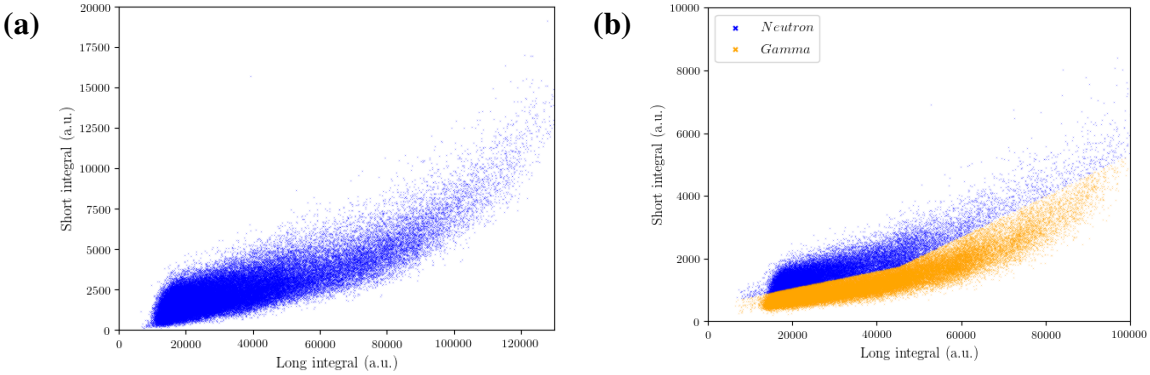

Figure 4. Comparison of CCM plots for the two plastic samples when exposed to ^{252}Cf and data were collected with 150 MS/s digitiser: a) Pixelated plastic and b) Cylindrical PSD plastic from LLNL.

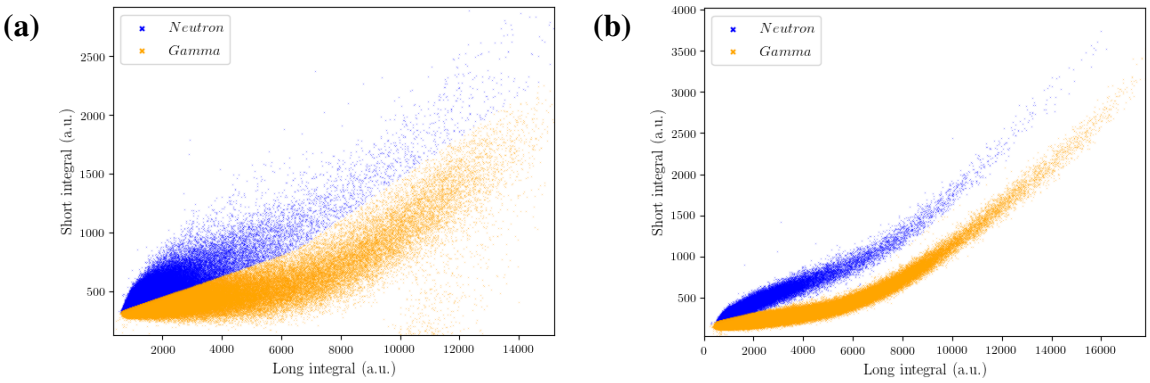

Figure 5. Comparison of CCM plots for the two plastic samples when exposed to ^{252}Cf and data were collected with 500 MS/s digitiser: a) Pixelated plastic and b) Cylindrical PSD plastic from LLNL.

3.1 Separation quality of each detector

The same data (i.e. as used to compose the scatter plots in figure 4 and figure 5) were used to assess the separation quality of each detector and signal digitiser arrangement. The figure-of-merit (FOM), as defined by eq. (3.1), was calculated for each case where the apparent separation quality was sufficient to meaningfully compare their performance. Neutron and gamma-ray events were separated through a discrimination line, as visible to the naked eye [21, 23], and were subsequently used to compose the coloured scatter PSD plots.

$$\text{FOM} = \frac{\text{Peak separation}}{\text{FWHM}_g + \text{FWHM}_n} \tag{3.1}$$

Peak separation in eq. (3.1) represents the distance between the peaks of the normal distribution fitting of neutron and gamma-ray plumes, while FWHM represents the full-width at half-maximum for each particle distribution. A Poisson approximation of the distribution was assumed in order to determine the corresponding uncertainty. Illustrative neutron and gamma-ray distribution plots in regard to the discrimination line are presented in figure 6, where the peak separation and FWHM for gamma-rays (FWHM$_g$) and neutrons (FWHM$_n$) are also shown.

The normal distribution fittings of neutron and gamma-ray plumes for the plots presented in figure 5, where data were collected using 500 MS/s digitiser, are presented in 7. As expected,

2019 JINST 14 P07017

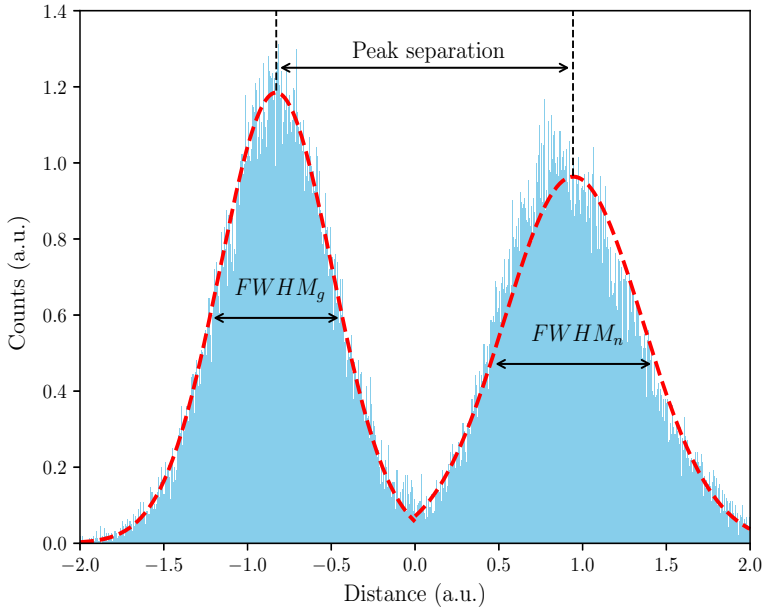

Figure 6. Example neutron and gamma-ray distribution in relation to the discrimination line, with the components of eq. (3.1) highlighted.

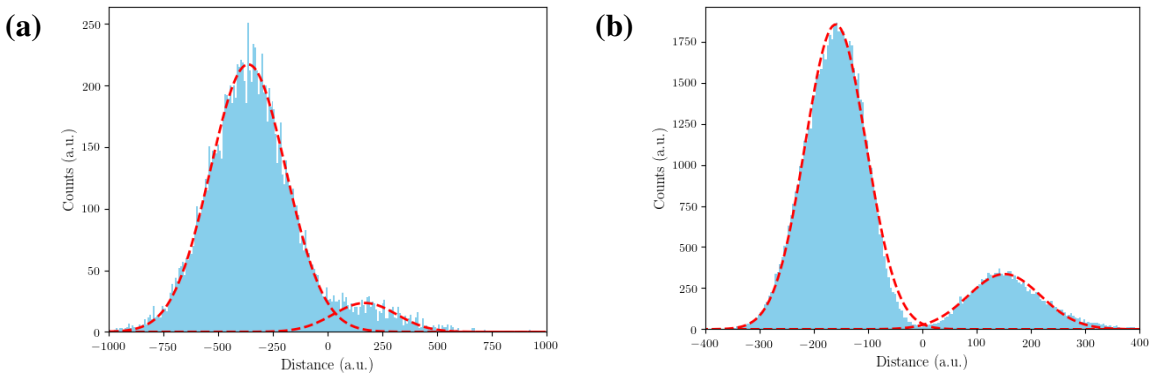

Figure 7. Comparison of neutron and gamma-ray distribution plots for the two plastic scintillators when exposed to ^{252}Cf and data were collected with 500 MS/s digitiser: a) Pixelated plastic and b) Cylindrical PSD plastic from LLNL.

the distributions in 7a are more widely spread across the distance from the distribution line when compared to the corresponding distribution in 7b. As a result, the number of counts for the PSD plastic is considerably higher, as the distribution is more condensed. This is in contrast to the lower number of counts for the pixelated plastic where the distance between the separation line and coordinates of the particle pulse is more varied.

The FOM values, together with corresponding statistical uncertainties calculated at the 95% confidence level, are presented in table 1. As the performance of the pixelated plastic scintillator with the 150 MS/s digitiser was insufficient to assume particle separation, FOM for this arrangement was not estimated. The FOM estimation results presented in table 1 reflect the relative quality of particle separation, as indicated qualitatively in figure 4 and figure 5. Despite the considerably

2019 JINST 14 P07017

Table 1. FOM values determined for each scintillator for the two digitisers used in this study.

Sample	Digitiser	FOM
PSD Plastic	150 MS/s	0.592 ± 0.001
	500 MS/s	0.637 ± 0.002
Pixelated plastic	150 MS/s	–
	500 MS/s	0.479 ± 0.010

lower FOM value in comparison to that of the cylindrical sample, the pixelated plastic scintillator in fact represents reasonable PSD performance in absolute terms. It should be noted that the pixelated scintillator was built in 2017 using Eljen Technology's old type PSD plastic EJ-299-34.

3.2 Pixelated scintillator performance with modulated neutron and gamma-ray fields

Based on the results presented above, it is apparent that the pixelated plastic scintillator (EJ-299-34) does not provide a clear neutron/gamma separation and the misclassification probability can be relatively high. Many factors can contribute to the overall PSD performance of a scintillator based detector, such as the energy spectrum of the radioactive isotope, the digitising electronics and photodetector type. These issues will be further considered in the following section 4. However, in order to first illustrate the particle separation performance of the pixelated scintillator in more depth, the mixed-field environment provided by ^{252}Cf was modulated.

The following three scenarios were considered to observe the detector's response to the modulated neutron and gamma-ray fields. In the first scenario, a 5 cm thick lead block was placed adjacent to the tank, between the source and the detector assembly, to reduce the number of gamma-ray photons reaching the scintillator. The thickness of the lead modulating block was subsequently doubled to 10 cm. The results of each scenario in the form of PSD scatter plots are presented in figure 8a and figure 8b, respectively. In the final arrangement, the neutron field was modulated by placing a HDPE block, of thickness 9 cm, adjacent to the tank between the radioactive source and the detector. Figure 8c illustrates the results obtained for this scenario. Distribution of neutron and gamma-ray photons in relation to the discrimination line, for the case of HDPE modulation, is presented in figure 8d. For each scenario, the detector was exposed to the radioactive field of ^{252}Cf for a duration of 30 mins.

4 Discussion

The PSD potential of a bespoke pixelated scintillator was experimentally tested. Building on the authors' prior work, the particle separation capability of the scintillator was first investigated using a FPGA based 150 MS/s digitiser [21, 27]. However, in this case, the pixelated plastic sample failed to separate neutrons from gamma-ray photons (figure 4a). Therefore, the performance of the digitiser was verified with a cylindrical PSD plastic scintillator sample, obtained from LLNL in 2016 and previously tested by the authors [21]. Results obtained with this cylindrical sample (figure 4b) indicate considerably superior performance, when compared with the pixelated plastic.

2019 JINST 14 P07017

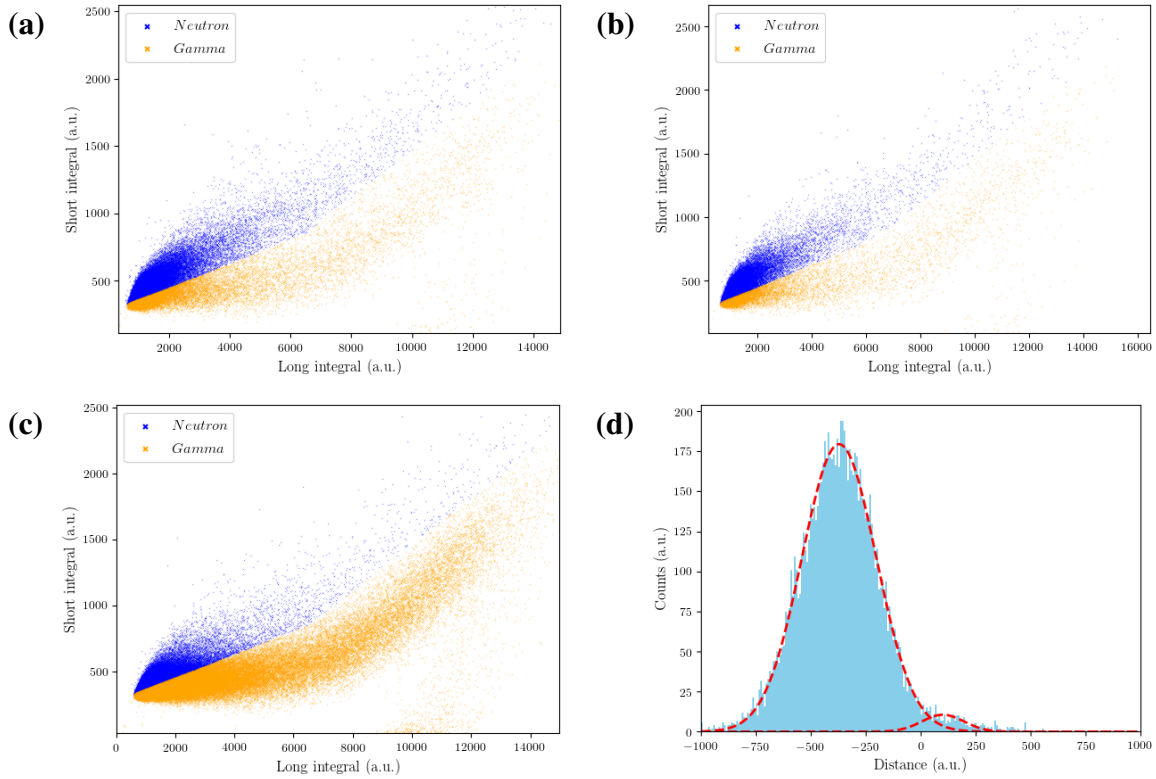

Figure 8. PSD scatter plots resulting from the exposure of the pixelated plastic scintillator detector to ^{252}Cf source with the following modulation type in place: (a) lead 5 cm, (b) lead 10 cm, (c) HDPE 9 cm and (d) neutron and gamma-ray distribution for HDPE modulated scenario.

Similar observations can be made for the experiments performed with a 500 MS/s digitiser. The pixelated plastic scintillator (EJ-299-34) shows considerably improved PSD performance when compared to the results obtained with the lower sampling rate digitiser. Although the estimated FOM of 0.457 is far from optimal, it was nonetheless possible to estimate FOM in this scenario, and the results demonstrate the promising PSD potential of the scintillator despite its small size and pixelated arrangement. As expected, the cylindrical research sample again shows improved PSD performance at this higher sampling rate, in comparison to the pixelated plastic sample, as evidenced by the FOM of 0.637 as well as figures 5b and 7b.

Dependence of PSD performance on the sampling rate of the digitising electronics has been previously discussed in literature [28]. Furthermore, new methods applied in the frequency domain suggest that digitisers of relatively low sampling frequency may be sufficient to separate neutrons from gamma-rays, when the digital data is considered in the frequency domain [29]. The results presented in this article suggest that there is a correlation between the sampling frequency of the digitiser and PSD performance measured using FOM, when PSD is performed in the time domain.

4.1 FOM as a measure of PSD performance

Particle separation performance between two particle types is often characterised by the FOM. It was first introduced by Winyard et al. [30], and further discussed by Knoll [3]. Although FOM is potentially a good measure of the separation quality, it should be used with caution since its

2019 JINST 14 P07017

value depends on the experimental context. It depends strongly on the low energy threshold, at which point the energy gate is defined [31]. The majority of organic scintillators present the highest misclassification probability in the low energy regions, and this decreases as the energy rises. In the present study, the energy gating was not considered, as the FOM estimation was performed across the whole energy spectrum.

Another important factor, which emerges as a part of this work, is the dependence of the FOM on the sampling frequency of the digitiser, when PSD analysis is performed in the time domain. It appears that if the intrinsic particle separation of a scintillator is sufficient, even the low sampling digitiser can be capable of performing satisfactory PSD. This is evidenced by comparing the PSD plots shown for the cylindrical sample in figure 4b and figure 5b. However, when the inherent PSD capabilities of a scintillator are not sufficient, as in the case of the pixelated EJ-299-34 scintillator, increased sampling rate provides significant improvement in terms of particle separation (figure 5a).

The estimated FOM value is also significantly impacted by the type of radioactive source used in a specific study, which is particularly important for organic scintillators aimed at fast neutron detection. The average energy of neutrons produced by the ^{252}Cf source is approximately 2.1–2.5 MeV, whereas neutrons produced by ^{241}AmBe average approximately 4.5 MeV. Moreover, the mixed field environment created by a radioisotope can be affected by the way it is stored. Since the neutron source used for the present work is stored in a water tank, the average energy spectrum of ^{252}Cf has been reduced to approximately 0.7–0.9 MeV [22]. This has further impact on the neutron/gamma separation in the low energy region.

Given the large number of factors contributing to the calculations of FOM, its value should always be interpreted on a case by case basis for specific research work or research environments. Many of the factors mentioned previously differ between research environments, and hence comparisons based purely on FOM do not reflect absolute differences between the quality of the results obtained.

4.2 Further assessment of the PSD quality in the pixelated plastic

As evidenced by the results presented in figure 5a, there exists a misclassification probability between neutrons and gamma-ray photons in the pixelated plastic scintillator. In contrast to the equivalent results obtained with the cylindrical PSD sample (figure 5b), there is no clear separation between the two particle types. There is noise present between the two plumes and the area of the lowest noise level was chosen to draw the separation line between the two particle types. As a single channel photodetector was used to collect the emitted fluorescence from a pixelated scintillator (where each block is optically isolated from one another), it is possible that the light collected in the photodetector is affected by interactions in more than one block of the scintillator.

Given the levels of noise present, the experiments performed with the pixelated plastic were repeated for three different scenarios when the ^{252}Cf mixed field environment was modulated. Firstly, the gamma-ray spectrum was modulated by placing 5 cm and 10 cm thick lead blocks adjacent to the tank between the source and the detector. The resulting plots are presented in figure 8a and figure 8b, respectively. As expected, the gamma-ray plume, which is presented in yellow, is significantly reduced in 8a and even more so in 8b.

Subsequently, 9 cm HDPE was used to modulate the neutron field, with the results presented in figure 8c. This time, the concentration of neutrons in the area of low integral values ($I_{\text{long}} \sim 2000$,

2019 JINST 14 P07017

$I_{short} \sim 750$) is noticeably reduced. The neutron concentration is higher in this region for the plot presented in figure 5a, where the results obtained with an unmodulated source are presented. With HDPE modulation, lower rates of neutron occurrences are also noticeable in the area of higher integral values ($I_{long} \sim 10000$, $I_{short} \sim 1500$). In a similar way the reduction of neutron count rate can be observed by the comparison of the distribution plots presented in 7a and 8d. There is a noticeable difference between the spread of neutron incidents across the distance axis as well as the number of counts, when the two plots are contrasted. The results discussed in this section further support the claim that the designed pixelated scintillator presents good PSD potential despite the intrinsically low PSD performance of the scintillator, when tested in this specific environment.

The neutron/gamma separation performance of EJ-299-34 has been previously assessed for larger scintillator blocks [32, 33]. The values of the estimated FOM quoted in these studies ($\sim$ 1.4–1.5) are considerably higher than the 0.479 reported in the present work. It should be noted that the testing conditions (radioactive source, digitiser, etc.) were different from one another, and from the scenario described in this paper. These earlier studies both utilised larger size scintillator blocks and the ratio of the number of photodetector channels to the number of pixels attached was smaller i.e. either 1:1 [32] or 1:16 [33].

It should also be mentioned that EJ-299-34 was originally described by Eljen Technology as a scintillator that was easier to form into array blocks due to the specific plastic content. Its PSD performance was deemed inferior to the EJ-299-33 plastic that was also available from Eljen at the same time, but not recommended for array applications. However, numerous studies have since shown that its PSD performance is relatively poor (especially in the low energy region) [34, 35], and remained inferior to equivalent liquid PSD capable scintillators [36]. It is, therefore, believed that the development of new plastics, whose PSD performance is comparable to liquid equivalents, would directly improve the performance of a small pixelated plastic scintillator, similar to the one presented in this work [7].

5 Conclusions

This article has reported on new experiments to investigate the PSD performance of a pixelated plastic scintillator. To the authors knowledge, this represents the first time that experimental results for the PSD of a pixelated plastic scintillator of this size have been presented. Despite the small size of individual pixels, the scintillator exhibits promising PSD results. It is believed that with improved inherent PSD for the scintillator material, the overall performance of a similarly designed scintillator would be further improved. In future research, therefore, it would be of great interest to test similar arrays built of the new plastic available from Eljen Technology (EJ-276).

It is also apparent that the photodetector used in this study does not provide optimal fluorescence collection for the pixelated plastic. As a single channel is responsible for light collection from the complete 13 $\times$ 13 array, there is a high probability of signal noise, due to interference from neighbouring pixels. It is, therefore, expected that replacing a single channel PMT with readily available pixelated photodetectors (PSPMT, SiPM) would help to alleviate these issues.

Moreover, with the advancement in the development of high speed digitisers, devices of 1 GS/s to 5 GS/s are now becoming available. Given the results obtained with the digitisers in this study, it is anticipated that an improved PSD would be observed, if higher sampling rate digitisers were

2019 JINST 14 P07017

used. It would also be advisable to gain more insight into the relationship between the particle separation quality and energy spectrum of the radioactive source. This could be tested by exposing the pixelated scintillator to other mixed-field environments, which provide different energy spectra, such as an unmoderated ^{252}Cf or ^{241}AmBe.

Acknowledgments

The authors would like to acknowledge the funding support from EPSRC (EP/M507891/1 and EP/R02572X/1), the Faculty of Science and Technology (Lancaster University, U.K.) and Sellafield Ltd. The authors would like to express their gratitude to Dr. Natalia Zaitseva and the team at LLNL for providing the plastic scintillator sample. The authors also acknowledge the use of the Matplotlib package for all plots presented in this paper [37].

References

[1] E.H. Lehmann and W. Wagner, *Neutron imaging at PSI: A promising tool in materials science and technology*, *Appl. Phys.* **A 99** (2010) 627.

[2] C.W.E. van Eijk, *Inorganic scintillators in medical imaging*, *Phys. Med. Biol.* **47** (2002) R85.

[3] G.F. Knoll, *Radiation Detection and Measurement*, 4th edition, John Wiley & Sons, Hoboken (2010).

[4] A. Kaplan, M. Flaska, A. Enqvist, J. Dolan and S. Pozzi, *EJ-309 pulse shape discrimination performance with a high gamma-ray-to-neutron ratio and low threshold*, *Nucl. Instrum. Meth.* **A 729** (2013) 463.

[5] M.J. Joyce, M.D. Aspinall, F.D. Cave and A.D. Lavietes, *Real-time, digital pulse-shape discrimination in non-hazardous fast liquid scintillation detectors: Prospects for safety and security*, *IEEE Trans. Nucl. Sci.* **59** (2012) 1245.

[6] L. Stevanato, D. Cester, G. Nebbia and G. Viesti, *Neutron detection in a high gamma-ray background with EJ-301 and EJ-309 liquid scintillators*, *Nucl. Instrum. Meth.* **A 690** (2012) 96.

[7] N.P. Zaitseva et al., *Recent developments in plastic scintillators with pulse shape discrimination*, *Nucl. Instrum. Meth.* **A 889** (2018) 97.

[8] F. Pino, L. Stevanato, D. Cester, G. Nebbia and G. Viesti, *Detecting fast and thermal neutrons with a boron loaded liquid scintillator, EJ-339A*, *Appl. Radiat. Isot.* **92** (2014) 6.

[9] N. Zaitseva et al., *Pulse shape discrimination with lithium-containing organic scintillators*, *Nucl. Instrum. Meth.* **A 729** (2013) 747.

[10] N. Zaitseva et al., *Scintillation properties of solution-grown trans-stilbene single crystals*, *Nucl. Instrum. Meth.* **A 789** (2015) 8.

[11] F.D. Becchetti et al., *Deuterated stilbene (stilbene-d12): An improved detector for fast neutrons*, *Nucl. Instrum. Meth.* **A 908** (2018) 376.

[12] M.M. Bourne, C. Mussi, E.C. Miller, S.D. Clarke, S.A. Pozzi and A. Gueorguiev, *Characterization of the CLYC detector for neutron and photon detection*, *Nucl. Instrum. Meth.* **A 736** (2014) 124.

[13] U. Shirwadkar et al., *Multi-Signature Composite Detector System for Nuclear Non-proliferation*, *IEEE Nucl. Sci. Symp. Med. Imag. Conf.* (2017) 1.

2019 JINST 14 P07017

[14] R. Accorsi, *Design of Near-Field Coded Aperture Cameras for High-Resolution Medical and Industrial Gamma-Ray Imaging*, (2001) [https://dspace.mit.edu/handle/1721.1/8684].

[15] E. Del Monte et al., *An X-ray imager based on silicon microstrip detector and coded mask*, *Nucl. Instrum. Meth.* **A 576** (2007) 191.

[16] O. Gal et al., *Development of a portable gamma camera with coded aperture*, *Nucl. Instrum. Meth.* **A 563** (2006) 233.

[17] M. Gmar et al., *Development of coded-aperture imaging with a compact gamma camera*, *IEEE Trans. Nucl. Sci.* **51** (2003) 1052.

[18] M. Jeong, B. Van, B.T. Wells, L.J. D'Aries and M.D. Hammig, *Scalable gamma-ray camera for wide-area search based on silicon photomultipliers array*, *Rev. Sci. Instrum.* **89** (2018) 033106.

[19] P. Hausladen, J. Newby, F. Liang and M. Blackston, *A Deployable Fast-Neutron Coded-Aperture Imager for Quantifying Nuclear Material*, Technical Report (2013).

[20] C.V. Griffith, R.S. Woolf and B.F. Phlips, *64-element fast-neutron, coded-aperture imager*, in *2017 IEEE International Symposium on Technologies for Homeland Security*, HST 2017, 2017, pp. 1–5 [DOI:10.1109/THS.2017.7943453].

[21] M.J. Cieślak, K.A.A. Gamage and R. Glover, *Pulse shape discrimination characteristics of stilbene crystal, pure and ^{6}Li loaded plastic scintillators for a high resolution coded-aperture neutron imager*, 2017 *JINST* **7** P07023.

[22] M.J. Cieślak, K.A.A. Gamage and R. Glover, *Investigation into a suitable scintillator and coded-aperture material for a mixed-field radiation imaging system*, 2017 *JINST* **12** P12007.

[23] K.A.A. Gamage, M.J. Joyce and N.P. Hawkes, *A comparison of four different digital algorithms for pulse-shape discrimination in fast scintillators*, *Nucl. Instrum. Meth.* **A 642** (2011) 78.

[24] M. Nakhostin, *A comparison of digital zero-crossing and charge-comparison methods for neutron/γ-ray discrimination with liquid scintillation detectors*, *Nucl. Instrum. Meth.* **A 797** (2015) 77.

[25] F. Brooks, *A scintillation counter with neutron and gamma-ray discriminators*, *Nucl. Instrum. Meth.* **4** (1959) 151.

[26] M.J. Cieślak, K.A.A. Gamage, R. Glover and C.J. Taylor, *Gamma-ray modulation properties of tungsten coded apertures for a novel mixed-field imaging system*, 2019 *JINST* **2** P02007.

[27] M.J.I. Balmer, K.A.A. Gamage and G.C. Taylor, *Neutron assay in mixed radiation fields with a ^{6}Li-loaded plastic scintillator*, 2015 *JINST* **10** P08012.

[28] M. Flaska, M. Faisal, D.D. Wentzloff and S.A. Pozzi, *Influence of sampling properties of fast-waveform digitizers on neutron-gamma-ray, pulse-shape discrimination for organic scintillation detectors*, *Nucl. Instrum. Meth.* **A 729** (2013) 456.

[29] M. Nakhostin, *Digital discrimination of neutrons and γ-rays in liquid scintillation detectors by using low sampling frequency ADCs*, *Nucl. Instrum. Meth.* **A 916** (2019) 66.

[30] R. Winyard, J. Lutkin and G. McBeth, *Pulse shape discrimination in inorganic and organic scintillators. I*, *Nucl. Instrum. Meth.* **95** (1971) 141.

[31] I. Pawełczak, S. Ouedraogo, A. Glenn, R. Wurtz and L. Nakae, *Studies of neutron-γ pulse shape discrimination in EJ-309 liquid scintillator using charge integration method*, *Nucl. Instrum. Meth.* **A 711** (2013) 21.

[32] J. Newby, P. Hausladen, M. Blackston and J.F. Liang, *Performance of Fast-Neutron Imaging Detectors Based on Plastic Scintillator*, ORNL/TM-2013/82, Oak Ridge National Laboratory (2013).

2019 JINST 14 P07017

[33] C. Payne et al., *Neutron/gamma pulse shape discrimination in EJ-299-34 at high flux*, *IEEE Nucl. Sci. Symp. Med. Imag. Conf.* **2016** 1.

[34] C. Liao and H. Yang, *Pulse shape discrimination using EJ-299-33 plastic scintillator coupled with a Silicon Photomultiplier array*, *Nucl. Instrum. Meth.* **A 789** (2015) 150.

[35] S. Chung, A. Kacperek, R. Speller and A. Gutierrez, *Optimisation of pulse shape discrimination using EJ299-33 for high energy neutron detection in proton beam therapy*, 2017 *JINST* **12** C11033.

[36] S.A. Pozzi, M.M. Bourne and S.D. Clarke, *Pulse shape discrimination in the plastic scintillator EJ-299-33*, *Nucl. Instrum. Meth.* **A 723** (2013) 19.

[37] J.D. Hunter, *Matplotlib: A 2D Graphics Environment*, *Comput. Sci. Eng.* **9** (2007) 90.

2019 JINST 14 P07017